Research Article

INDONESIAN SCHOLAR SOCIETY

Indones. J. Chem. Stud.
2026, 5(1), 83–89
Available online at journal.solusiriset.com
e-ISSN: 2830-7658; p-ISSN: 2830-778X

Indonesian Journal of Chemical Studies

Transformation of Rusty Iron as a TiO_2 Dopant for CO Photodegradation of Jepara Furniture Wooden Oven Exhaust

Syafriyanti Annur[1]*, Syarifa Rizka Kautsari[1], Reysha Camila Iffatul Amalia[1]

[1]MAN 1 Jepara, Bawu, Batealit, Jepara 59461, Indonesia

Received: 5 May 2026; Revised: 25 Jun 2026; Accepted: 29 Jun 2026;
Published online: 30 Jun 2026; Published regularly: 30 Jun 2026

Abstract— The furniture industry in Jepara utilizes wood-fired ovens that generate exhaust emissions containing carbon monoxide, which pose potential risks to both the environment and public health. One promising approach to reducing CO emissions is the application of TiO_2 photocatalysts, whose photocatalytic performance can be enhanced through Fe doping using an environmentally friendly Fe source derived from rusty iron waste. TiO_2 photocatalysts can be applied in the form of coatings. This study aimed to analyze the Fe content of rusty iron waste, synthesize and characterize TiO_2-Fe, develop a prototype test chamber for TiO_2-Fe coating application, and evaluate its effectiveness in reducing CO emissions from wood-fired oven exhaust. X-ray fluorescence (XRF) analysis revealed that rusty iron waste contained 99.49% Fe (as total Fe content), demonstrating its suitability as a dopant source for TiO_2-Fe synthesis. TiO_2-Fe was synthesized using Fe:TiO_2 mass ratios of 1:2, 1:1, and 2:1. Scanning electron microscopy (SEM) analysis showed that the 1:1 mass ratio produced smaller particles with a more homogeneous distribution and lower agglomeration, while UV–Vis diffuse reflectance spectroscopy (SR-UV) analysis indicated the greatest reduction in band gap energy, from 3.2 eV to 2.8 eV. Application of the TiO_2-Fe coating in the prototype test chamber achieved a maximum degradation efficiency of 81.8% under visible-light irradiation, outperforming both commercial coatings and TiO_2-$FeCl_3$ coatings. These findings demonstrate that TiO_2-Fe derived from rusty iron waste has significant potential as a functional photocatalytic material for mitigating air pollution.

Keywords— *Carbon monoxide; Iron rust; Photocatalyst; Woof-fired oven*

1. INTRODUCTION

Jepara Regency, Central Java Province, is famous for its flagship products, one of which is furniture. This is evident from the number of workers and business operators employed by the furniture industry. Based on BPS-Jepara Regency, there are 237 units of wood furniture industry in Jepara Regency. The well-known products of the Jepara furniture industry include tables, chairs, cabinets, kitchen sets, buffets, and doors. Before manufacturing these products, the wood to be used is dried by removing its moisture content in a wood-fired oven at an average temperature of 100°C. Many wood furniture industries in Jepara have wood-fired ovens. These wood-fired ovens use firewood as their heat source. The smoke contains carbon monoxide (CO) at concentrations of approximately 500–700 ppm [1]. The emissions from the wood-fired oven chimneys are released into the atmosphere without any treatment.

Carbon monoxide (CO) is a toxic gaseous pollutant. When inhaled by humans, carbon monoxide can cause respiratory problems. This is because CO binds to hemoglobin in the body, thereby disrupting the delivery of oxygen throughout the body [2]. In addition, CO can also cause cardiovascular disease, acute kidney failure, hypertension, acute brain injury, brain lesions, decreased lung capacity, tissue hypoxia, and low birth weight (LBW). Currently, the public still has limited information regarding solutions to reduce carbon monoxide (CO) levels; therefore, further research and development are needed. In this study, the researchers will reduce the carbon monoxide content in wood furniture oven emissions using a photocatalyst with iron rust waste as the dopant source.

A photocatalyst is a catalyst that can accelerate chemical reactions using light. Photocatalysis is a process that combines photochemistry and catalysis. Materials that can be used in photocatalytic processes include semiconductors such as TiO_2, ZnO, Fe_2O_3, CdS, GaP, ZnS, and WO_3 [3]. This study uses TiO_2 as a catalyst because it has large pores and a high specific surface area, is inexpensive, abundant in nature, non-toxic, and stable under light. However, it has a limitation in that it cannot absorb radiation beyond the UV range (λ <388 nm). Therefore, to enhance the catalyst's performance by improving its ability to absorb visible light wavelengths, the TiO_2 material was modified by incorporating iron rust waste into the TiO_2composition. Common Fe sources used as dopants typically come from expensive commercial materials such as $FeCl_3$, $FeNO_3$, and $Fe(C_5H_7O_2)$ [3]; in this study, an

***Corresponding author**.
Email address: syafrimansara@gmail.com
DOI: 10.55749/ijcs.v5i1.182

environmentally friendly Fe source is used, namely inexpensive and abundant rusted iron. The purpose of using Fe from rusted iron is to implement a green chemistry approach in terms of the materials used.

The coprecipitation method was chosen in this study because of its advantages over other synthesis methods. Unlike sol-gels and solvothermals that require strict temperature and pressure control and the use of complex precursors, or solid-state methods that require high calcination temperatures that are energy-consuming, coprecipitation can be performed at low temperatures with simple equipment, affordable costs, and relatively short synthesis times [4]. Meanwhile, the synthesis of Fe-doped$TiO_2$was carried out using the solid-state reaction (SSR) method. The solid-state reaction method involves reacting one solid with another. The advantages of this method include an easy preparation process, simple equipment, and the ability to maintain phase purity [4]. Research on photocatalysts has been conducted by Xia, H et al. [5]. That study developed a waterborne coating of Fe/N/Co–TiO_2 to reduce CO content in vehicle exhaust. The study successfully reduced CO concentration by 25.20% under visible light. The study used multi-doping, which can lead to a decrease in photocatalyst efficiency. Therefore, an optimal dopant concentration is required so that the photocatalytic process achieves maximum degradation.

Given this background, the application of coatings to chimneys has never been done before. The novelty of this study lies in the creation of a TiO_2–Fe coating applied to chimneys from the exhaust of Jepara wood furniture ovens, which is expected to reduce CO. Additionally, the Fe we used was sourced from rusty iron waste, which is widely available in the environment. The objectives of this study are to analyze the Fe content of rusty iron waste, synthesize and characterize Fe-doped TiO_2 from rusty iron waste, create a prototype test chamber for applying the TiO_2-Fe coating, and study the effectiveness of the TiO2-Fe coating on the exhaust stack of a Jepara wooden furniture kiln.

2. EXPERIMENTAL SECTION

2.1. Materials

The materials used in this study were rusty iron waste, 37% hydrochloric acid (HCl), 25% ammonium hydroxide (NH_4OH), distilled water, titanium dioxide (TiO_2), ferric chloride ($FeCl_3$), water-based resin, and commercial coating.

2.2. Instrumentations

The equipment used in this study included an analytical balance, filter paper, watch glasses, funnels, an oven, 250 mL and 600 mL beakers, 100 mL and 500 mL Erlenmeyer flasks, a mortar, a pestle, pH indicator paper, a hot plate stirrer, a neodymium magnet, aluminum foil, a magnetic stirrer, a Scanning Electron Microscope (SEM), X-ray Fluorescence (XRF), and a Specular Reflectance UV-Visible Spectrophotometer (SR-UV).

2.3. Analysis and Characterization of Fe Content in Iron Rust Waste

This process consists of: sorting rusty iron waste using a magnet. Next, the rusty iron waste is dissolved in 37% hydrochloric acid (HCl) at a temperature of 70°C for 1 hour, after which the iron (Fe) solution is filtered twice using filter paper. Next, 25% ammonium hydroxide (NH_4OH) is added until a pH of 5 is reached using a hot plate. The iron (Fe) solution is neutralized with distilled water. It is then dried in an oven at 115°C for 90 minutes. Finally, it is ground in a mortar to form a powder. In the next step, the iron(III) oxide (Fe_2O_3) powder was calcined at 600°C for 1 hour. The percentage composition of the iron(III) oxide (Fe_2O_3) powder can be determined using XRF (X-ray fluorescence) analysis.

2.4. Synthesis and Characterization of TiO2-Fe Photocatalysts from Iron Rust

The resulting iron(III) oxide (Fe_2O_3) powder was then mixed with TiO_2 in ratios of 1:2, 1:1, and 2:1. The mixture was ground for 2 hours until homogeneous. Next, a calcination process was carried out at 500°C for 3 hours. After calcination, the material was ground again to break up clumps and obtain a finer result. Subsequently, to observe the morphology and particle size, characterization was performed using Scanning Electron Microscopy (SEM), while UV Vis Reflectance Spectroscopy (SR-UV) was used to observe shifts in absorption wavelengths and evaluate changes in the bandgap energy (Eg) resulting from Fe doping in TiO_2 under various ratios. Additionally, TiO_2-Fe was synthesized from TiO_2-$FeCl_3$ using a 1:1 ratio of s as a reference (control).

2.5. Designing a Test Chamber Prototype

The test chamber prototype was designed by researchers using AutoCAD Inventor. The resulting design was then engineered and fabricated in-house with the assistance of craftsmen, based on the findings of the literature review. The design of the apparatus was scaled down to laboratory size, as furniture wood ovens are generally larger **Fig. 1**.

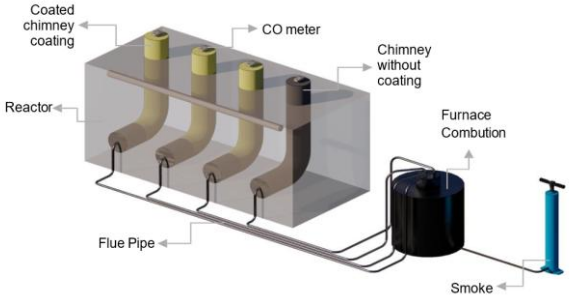

Fig. 1. Design of the test chamber prototype

The design consists of several components: a chimney, a reactor box, a smoke hose, a combustion chamber, and a smoke pump. The resulting test chamber is shown in **Fig. 2.**

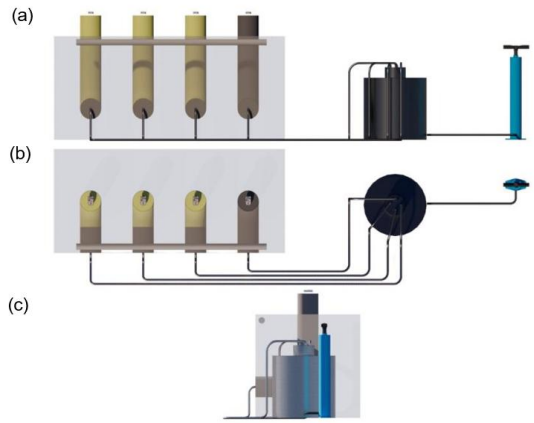

Fig. 2. Overall view of the test chamber prototype: (a) front view, (b) top view, and (c) side view

Meanwhile, to ensure the uniformity of the CO gas output, the flow rate was calculated using **Eq. (1)**. Where Q is gas flow rate (m^3/s), A is cross-sectional area of the chimney (m^2), s is distance traveled by the gas over time (m), and t is time the gas is in motion (s).

$$Q = \frac{\mathrm{A\ x\ s}}{\mathrm{t}} \quad (1)$$

2.6. Application of TiO_2-Fe

The coating application process was carried out using various TiO_2–Fe materials prepared in three mass ratios: 1:2, 1:1, and 2:1. Each composition was mixed with a water-based resin and distilled water to produce a homogeneous solution. The solution was then applied as a coating to the chimney surface inside the test chamber. After the coating process was complete, carbon monoxide (CO) concentration measurements were taken using a CO meter to determine the effectiveness of the TiO_2–Fe coating in reducing CO emissions. The amount of carbon monoxide degraded (in %) was calculated using **Eq. (2).** Where Co is initial carbon monoxide concentration and Cf is final carbon monoxide concentration

$$\%\mathrm{Degraded} = \frac{Co-Cf}{Co} \times 100\% \quad (2)$$

This process was repeated three times. The following controls were used in this study: an uncoated chimney, a chimney coated with a commercial coating, and a chimney coated with a TiO_2–$FeCl_3$ coating. The application process was conducted under sunlight (exposed to visible light) and compared to conditions in the dark.

3. RESULT AND DISCUSSION

3.1. Analysis and Characterization of Fe Content in Iron Rust Waste

The iron rust waste used in this study was collected from rusted iron around MAN 1 Jepara. The synthesis of Fe2O3 was carried out using the coprecipitation method. This method was chosen because it is the simplest, most efficient, and most economical. The iron rust waste was sorted to separate it from impurities and other materials. Next, dissolution with 37% HCl was performed to dissolve the Fe present in the iron rust **Fig. 3.** The reaction that occurred during this process can be described in **Eq. (3).**

$$Fe_2O_3(s) + 6HCl(aq) \rightarrow 2FeCl_3(aq) + 3H_2O(l) \quad (3)$$

The solution is filtered to remove impurities. 25% NH_4OH is added to the filtered solution and stirred using a magnetic stirrer until the pH reaches 5. This process produces a precipitate and results in **Eq. (4).**

$$2FeCl_3(l) + 3H_2O(l) + 6NH_4OH(l) \rightarrow 2Fe(OH)_3(s) + 6NH_4Cl(l) + 3H_2O(l) \quad (4)$$

Next, the sample is washed with distilled water to neutralize the solution and remove any remaining HCl and impurities from the precipitate. The precipitate is placed in an oven to remove moisture from the sample, resulting in **Eq. (5).**

$$2Fe(OH)_3(s) + 6NH_4Cl(l) + 3H_2O(l) \rightarrow 2FeOOH + 6NH_4Cl(l) + 5H_2O(l) \quad (5)$$

In the next step, the iron(III) oxide (Fe_2O_3) powder is calcined, resulting in **Eq. (6).**

$$2FeOOH(s) + 6NH_4Cl(l) + 5\ H_2O(l) \rightarrow Fe_2O_3(s) \quad (6)$$

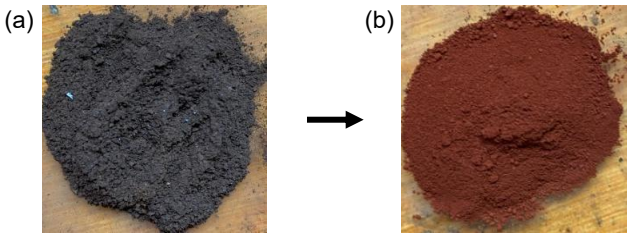

Fig. 3. Rusty iron waste (a) before and (b) after the coprecipitation process

Next, to determine the percentage of elemental content in iron(III) oxide (Fe_2O_3) powder, testing was conducted using the X-ray fluorescence (XRF) method. This analysis aimed to confirm the presence of Fe_2O_3 and determine the total iron content in the rusty iron waste. The XRF analysis results are presented in **Table 1.** the rusty iron waste shows a dominance of Fe with a concentration of 99.49%. These results indicate that this material has a high metal content and has potential as a feedstock for the synthesis of photocatalytic materials. Meanwhile, other elements such as Cr, Zn, Sn, and Pb

Table 1. Elemental composition of iron rust waste based on XRF test results

Element	Content (%)
Fe	99.49
Cr	0.082
Zn	0.103
Sn	0.035
Pb	0.29

are likely derived from residues of the rusty iron dredging process. Low-concentration metals (<1%) do not affect the effectiveness of the Fe doping process into TiO_2, as low concentrations generally do not have a significant impact on either the Fe doping process or the TiO_2 crystal structure.

3.2. Synthesis and Characterization of TiO_2-Fe Photocatalysts from Iron Rust

In the synthesis of TiO_2–Fe using the solid-state reaction method, since it does not require additional solvents and is classified as a green synthesis method [4]. Fe and TiO_2 mixed in mass ratios of 1:2, 2:2, and 2:1 were \then ground to create a homogeneous material and maximize the interaction between Fe and TiO_2. After grinding, the mixture was calcined to optimize formation, resulting in the best possible material. The resulting TiO_2–Fe material was then analyzed using Scanning Electron Microscopy (SEM) to observe surface morphology and particle size. Observations were conducted on samples at a magnification of 10,000x. The SEM results are shown in **Fig. 4.**

Based on **Fig. 4.,** the results of SEM analysis at 10,000x magnification show the presence of particle agglomeration, which is the process of nano-sized particles combining to form larger structures [6]. In **Fig. 4. (c)**, the agglomeration level is lower than in other samples, so the material has a larger surface area. A large surface area plays a crucial role in enhancing photocatalytic performance by providing more active sites that support the photodegradation process. This is consistent with the research by Mohtar et al. (2021) [7]. Meanwhile, **Fig. 4(a), 4(b),** and **4(d)** show particles that tend to be larger and clumped together, indicating a higher degree of agglomeration. This condition results in a reduced surface area, thereby decreasing the number of active sites and lowering the photocatalyst's effectiveness compared to the sample in **Fig. 4(c)**.

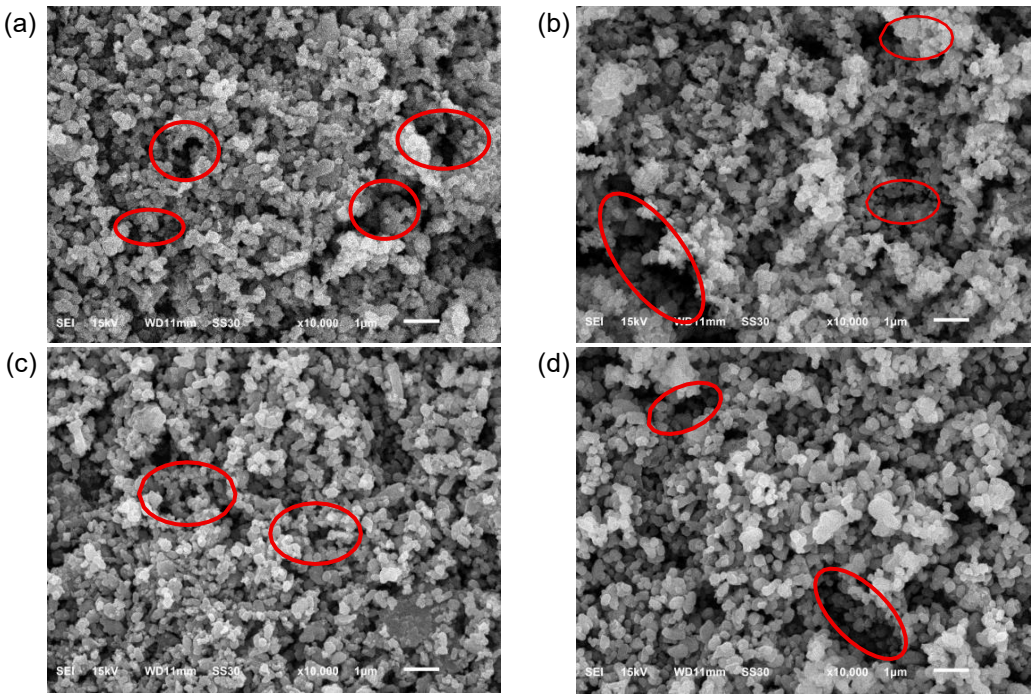

Fig. 4. SEM images of (a) TiO_2–Fe (2:1), (b)TiO_2–Fe (1:2), (c) TiO_2–Fe (1:1), and (d) TiO_2

Next, to determine the band gap value, SR-UV analysis was performed. The results of the analysis are shown in **Table 2.** UV light has a wavelength range of 100–400 nm, while visible light falls within the range of 400–750 nm. **Table 2.** shows that Fe doping causes a wavelength shift toward the visible light region (greater than 400 nm). This is consistent with the research by Mancuso et al. [8].

In addition, there was a decrease in the Eg value of TiO_2 from 3.2 eV to 3.1–2.2 eV in Fe-doped TiO_2. Based on research by Wahyuni et al. [9], the optimal Eg range is approximately 2.4–2.8 eV, as it provides good visible optimal Eg value can increase the photocatalyst activity under exposure to visible light by shifting the wavelength towards the visible light so that the percentage of CO degradation is more optimal. Based on **Table 2.**, it can be observed that Fe-doped TiO_2 with a 1:1 mass ratio yields an optimal Eg value of 2.8 eV. For the TiO_2:Fe mass ratio of 1:2, an Eg value 3.0 eV, indicating that an excess of TiO_2 can reduce the available active surface area of the catalyst [10].

Table 2. Bandgap energy and wavelength values for TiO_2 and TiO_2-Fe photocatalysts

Material	λ (nm)	Eg (eV)
TiO_2	388	3.2
TiO:Fe (2:1)	402	3.1
TiO:Fe (1:1)	442	2.8
TiO:Fe (1:2)	556	2.2

3.3. Construction of a Test Chamber for Jepara Wooden Furniture Ovens

The test chamber prototype consists of several materials, namely: galvanized steel for the reactor box, which measures 100 cm x 50 cm x 60 cm and serves as the outer layer of the chimney to protect against smoke and moisture exposure during the process. There is also a 6 cm diameter steel pipe serving as the chimney, coated with a protective layer, and a 3 cm diameter steel pipe, 150 cm long, which functions as the inlet for smoke from the wood-burning furnace into the reactor box. The wood-burning stove, measuring 40 cm x 40 cm x 43 cm, serves as the primary source of g s and is used to burn wood, producing smoke. Additionally, a smoke pump is used to force the smoke out of the stove into the reactor chamber. A CO meter is the instrument used to measure the concentration of carbon monoxide (CO) produced. The test chamber prototype can be seen in **Fig. 5.**

Fig. 5. Test chamber prototype

The uniformity of the CO gas output was determined by calculating the average flow rate from each chimney. The calculation results are shown in **Table 3.** The average CO gas flow rate measurements from the four stacks yielded relatively uniform values, with an overall average of 7.63 × 10^−4m³/s and a significance value of 0.999 (p > 0.05), indicating that there is no significant difference between the average flow rates of the four chimneys. These results indicate that the CO gas emitted from the four chimneys has a relatively similar flow rate, suggesting that the chimneys operate uniformly in discharging the gas.

Table 3. Flue gas flow rates in the test chamber (n=3)

Chimney	Average
1	7.63×10^{-4}
2	7.63×10^{-4}
3	7.65×10^{-4}
4	7.61×10^{-4}
Average	7.63×10^{-4}
F	0.005
Sig.	0.999

3.4. Results of TiO_2-Fe Application for CO Degradation

TiO_2-Fe photocatalyst was applied as a coating on the chimneys of Jepara wooden furniture kilns with the aim of reducing the levels of carbon monoxide (CO) produced during the combustion process. The testing process was conducted by igniting the wood-burning furnace until smoke was produced; the smoke was then pumped through a hose into four chimneys, each of which had been coated. Additionally, a control chimney was used to compare the effectiveness of the synthesized TiO_2-Fe photocatalyst with TiO_2-$FeCl_3$, an uncoated chimney, and a commercial coating. At the end of the chimney, the CO level is measured using a CO meter. The CO meter works by inserting the probe tip into the end of the smoke chimney so that the resulting emission levels can be detected by the device, allowing for the observation of the effectiveness of TiO_2-Fe in the combustion produced by the wood-fired oven.

The mechanism of CO degradation by TiO_2-Fe photocatalyst coating goes through several stages. In the first stage, the coating is exposed to visible light so that the electrons in the valence band are detected towards the conduction band and leave a hole in the valence band, the presence of Fe doping helps to suppress the electrone-hole pair recombination and expand the absorption of light towards the visible beam, thus increasing the photocatalytic efficiency. The second stage, i.e. the electrons produced in the previous stage react with the oxygen adopted on the catalyst surface to form superoxide radicals ($O_2^{\bullet-}$), while the hole reacts with hydroxide ions or water that is absorbed to form hydroxyl radicals (•OH). The third stage is the adsorbtion of CO at the active site of the coating surface. The next stage is CO oxidation, where the adopted CO reacts with hydroxyl and superoxide radicals to become CO_2. The last stage is the desorption of CO_2 from the coating surface, so that the active site is empty again.

CO degradation reactions are included as heterogeneous photocatalytic oxidation reactions. This reaction is photoinduced by utilizing the formation of an electrone-hole pair due to light absorption to produce a reactive oxygen species that oxidizes CO into CO_2 in **Eq. (7)**. Dopan Fe in TiO_2 coating functions to increase charge carrier recombination, so that CO degradation is more optimal compared to TiO_2 coating without doping.

$$2CO(g) + O_2(g) \rightarrow 2CO_2(g) \quad (7)$$

3.4.1. The effect of variations in TiO_2–Fe mass on CO degradation efficiency

Photodegradation of CO using Fe-doped TiO_2 coatings was conducted with different mass variations, applied under dark conditions and under visible light exposure. The results of the percentage of CO degraded are shown in **Fig. 6.**

The 1:1 TiO_2–Fe mass ratio yields the most optimal CO degradation efficiency under visible light exposure at 85.2%, compared to the 2:1 and 1:2 mass ratios. In the 1:1 mass ratio, the balanced mass ratio between Fe and TiO_2maximizes light absorption, thereby making the CO

degradation process more effective. In the 2:1 TiO_2–Fe ratio, the small amount of Fe results in suboptimal visible light absorption. This is because the amount of Fe dopant is insufficient to extend light absorption into the visible region. Conversely, in the 1:2 variation, the excessive amount of Fe actually covers part of the TiO_2 surface, causing reduced light absorption and lowering the effectiveness of the degradation process. This is consistent with the SEM and SRUV characterization results, as well as with previous research by Mancuso et al. [8].

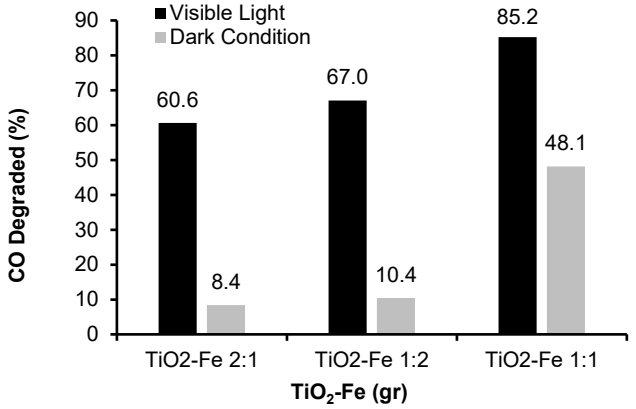

Fig. 6. Results of CO photodegradation efficiency using TiO_2–Fe coatings with varying mass fractions under visible light exposure and in the dark condition (n=3)

In addition, the data in **Fig. 6.** show that CO degradation is more effective under visible light exposure than in the dark. This is because light energy helps activate the TiO_2–Fe catalyst, whereas in the dark, the catalyst's performance decreases significantly [11].

3.4.2. Comparison of the effectiveness of the optimized TiO_2–Fe photocatalyst with undoped TiO_2, TiO_2–$FeCl_3$, and a commercial coating

The TiO_2–Fe photocatalyst with the optimal 1:1 mass ratio from the previous stage was then compared in terms of effectiveness against undopedTiO_2, TiO_2–$FeCl_3$, and a commercial coating.

The TiO_2–Fe 1:1 mixtureexhibits the highest CO degradation rate compared to the others. The commercial coating was only able to degrade 18.2% of the CO. Meanwhile, TiO_2 degrades CO by 52.5%, and TiO_2 $FeCl_3$ is capable of degrading it by 63.6%. This confirms that TiO_2–Fe exhibits the most effective performance in CO degradation. The data clearly indicate that undoped$TiO_2$is less effective, as the Fe content can cause a shift in the wavelength toward the visible light region, thereby increasing the available active surface area.

In addition, the concentration of CO resulting from degradation was calculated and compared with the maximum safe limit of 400 ppm, in accordance with the ANSI Z21.47 standard [12]. The results of this comparison with the standard limit are shown in **Fig. 8.**

The CO concentration did not exceed the safe limit in the TiO_2–Fe 1:1 mass ratio, which resulted in a concentration of 153.3 ppm. Meanwhile, in the other stack, the CO concentration exceeded the safe limit. These data reinforce that the TiO_2–Fe mass ratio of 1:1 is the most effective condition, as it not only exhibits the highest degradation percentage but also produces a CO concentration below the safe quality standard.

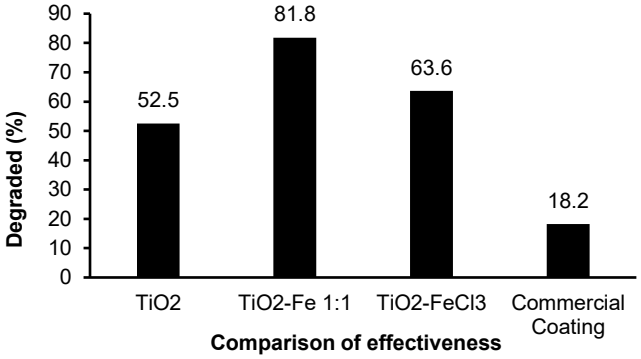

Fig. 7. Comparison of the effectiveness of various photocatalysts in CO degradation

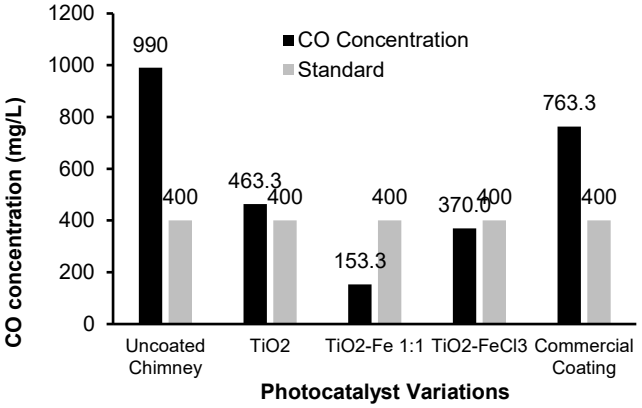

Fig. 8. Comparison of CO concentrations with quality standards for various coating variations

4. CONCLUSION

Based on the research conducted, it can be concluded that rusty iron waste can be recycled into Fe_2O_3 material using the coprecipitation method. XRF characterization shows that rusty iron waste contains Fe with a concentration of 99.49%, which can be used as a dopant source. The synthesis of Fe-doped TiO_2 was carried out using the solid-state reaction method. Analysis results using SEM at a 1:1 mass ratio showed smaller particle morphology, more homogeneous distribution, and lower agglomeration. Based on SR-UV testing, there was a decrease in the Eg value of TiO_2 from 3.2 eV to 3.1–2.2 eV in Fe-doped TiO_2. The most optimal Eg reduction was observed in the 1:1 mass ratio, at 2.8 eV. The test chamber prototype that has been constructed can be used to evaluate the effectiveness of the coating in the treatment of exhaust fumes from Jepara wooden furniture ovens. Based on the ANOVA test results, a significance value of 0.999 ($p > 0.05$) was obtained, indicating that there is no significant difference between the average

flow rates of the four chimneys. The efficiency of theTiO_2–Fe coating in reducing CO levels in oven flue gas is most optimal at a 1:1 mass ratio under visible light, with a degradation rate of 81.8%, outperforming the commercial coating (18.2%) and the TiO_2–$FeCl_3$ coating (63.6%). The 1:1 mass ratio of TiO_2–Fe showed that CO concentrations did not exceed the safe limit of 153.3 ppm (<400ppm).

5. AUTHOR'S DECLARATION

5.1. Supporting Information

This study does not include supporting materials.

5.2. Acknowledgements

The authors would like to express their sincere gratitude to the Mansara Research Club (MRC) at MAN 1 Jepara for the guidance, facilities, and support provided during the research process and the preparation of this scientific journal. The motivation, guidance, and conducive academic environment greatly contributed to the authors' success in completing this research.

5.3. Conflict of Interest

The authors declare that they have no financial or personal conflicts of interest regarding the publication of this journal.

5.4. Author Contributions

SA: Conceptualization, Project administration, Supervision, Validation, and Writing the original manuscript. RCIA: Conceptualization, Formal analysis, Project administration, Methodology, Investigation, Supervision, Validation, and Writing the original draft. SRK: Conceptualization, Formal analysis, Project administration, Methodology, Investigation, Supervision, Validation, and Writing the original draft.

5.5. AI Statement

ChatGPT was utilize to enhance the clarity, grammar, and overall readability of this manuscript. All technical content, data interpretation, and conclusion were solely developed and verified by the authors. The final version of the manuscript was thoroughly reviewed to ensure accuracy, coherence, and aligment with the study's findings.

6. REFERENCES

[1] Singh, D., Tassew, D. D., Nelson, J., Chalbot, M. C. G., Kavouras, I. G., Tesfaigzi, Y., Demokritou, P. 2022. Physicochemical and toxicological properties of wood smoke particulate matter as a function of wood species and combustion condition. *J. of Hazard. Mater.* 441. 129874. Doi: https://doi.org/10.1016/j.jhazmat.2022.129874

[2] Salma, A. L., Ernyasih. 2025. Tinjauan pajanan karbon monoksida (co) dan dampaknya terhadap kesehatan pedagang kaki lima di wilayah perkotaan padat lalu lintas. *EOHSJ. 5*(2). 85-96. Doi :https://doi.org/10.24853/eohjs.5.2.85-97

[3] Alaghmandfard, A. and Ghandi, K. 2022. A Comprehensive Review of Graphitic Carbon Nitride (g-C_3N_4)–Metal Oxide-Based Nanocomposites: Potential for Photocatalysis and Sensing. *Nanomaterials. 12*(2). 294. Doi: https://doi.org/10.3390/nano12020294

[4] Crismeli., Nurhidayah., Restianingsih T., Anggraini R.M., Deswardani F. 2024. Analysis of the Crystal Structure and Morphology of Fe3O4/TiO2Nanocomposites Based on Iron Sand from the Batanghari River. *Journal Online of Physics. 9*(2). 12–17. Doi: https://doi.org/10.22437/jop.v9i2.29661

[5] Xia, H., Liu, G., Zhang, R., Song, L., Chen, H. 2019. The Photocatalytic Degradation of Vehicle Exhausts by an Fe/N/Co–TiO_2Waterborne Coating under Visible Light. *Nat. Lib. of Med. 12*(20). 3378. Doi: https://doi.org/10.3390/ma12203378

[6] Melinia, L.A., Puspita, E., Naibaho, M., Ramlan, R. and Ginting, M. 2022. Analisis Pasir Besi Alam Dari Sungai Musi Sumatera Selatan. *Jurnal Penelitian Sains. 24*(3). 122-126. Doi: https://doi.org/10.56064/jps.v24i3.716

[7] Mohtar, S.S., Aziz, F., Ismail, A.F., Sambudi, N.S., Abdullah, H., Rosli, A.N. and Ohtani, B. 2021. Impact of Doping and Additive Applications on Photocatalyst Textural Properties in Removing Organic Pollutants: A Review. *Catalysts. 11*(10). 1160. Doi: https://doi.org/10.3390/catal11101160

[8] Mancuso, A., Sacco, O., Vaiano, V., Bonelli, B., Esposito, S., Freyria, F.S., Blangetti, N. and Sannino, D. 2021. Visible Light-Driven Photocatalytic Activity and Kinetics of Fe-Doped TiO2 Prepared by a Three-Block Copolymer Templating Approach. *Materials. 14*(11). 3105. Doi: https://doi.org/10.3390/ma14113105

[9] Wahyuni, E.T., Annur, S., Lestari, N.D. and Mudasir, M. 2024. Conversion of Iron Rusty Waste Into Fe Dopant of Tio2 to Increase its Photocatalytic Activity Under Visible Light for Photodegradation of Rhodamine-B. *Res. in Eng. 22.* Doi: https://doi.org/10.1016/j.rineng.2024.102296

[10] Moridon, S.N.F., Arifin, K., Yunus, R.M., Minggu, L.J. and Kassim, M.B. 2022. Photocatalytic water splitting performance of TiO_2 sensitized by metal chalcogenides: A review. *Ceramics Intl. 48*(5). 5892-5907. Doi: https://doi.org/10.1016/j.ceramint.2021.11.199

[11] Haque, F., Blanchard, A., Laipply, B. and Dong, X. 2024. Visible-Light-Activated TiO_2-Based Photocatalysts for the Inactivation of Pathogenic Bacteria. *Catalysts. 14*(12). 855. Doi: https://doi.org/10.3390/catal14120855

[12] CSA Group & American National Standards Institute. 2021. Gas-fired central furnaces. https://webstore.ansi.org/standards/csa/csaansiz2147212021